TÜBİTAK

Turkish Journal of Botany

http://journals.tubitak.gov.tr/botany/

Research Article

Turk J Bot
(2023) 47: 127-139
© TÜBİTAK
doi:10.55730/1300-008X.2751

Dynamics of CO_2 consumption, and biomass and lipid carbon production during photobioreactor cultivation of the diatom *Cyclotella*

Altan ÖZKAN*
Department of Environmental Engineering, Faculty of Engineering, İzmir Institute of Technology, İzmir, Turkey

Received: 09.09.2022 • **Accepted/Published Online:** 09.02.2023 • **Final Version:** 23.03.2023

Abstract: Understanding of CO_2 delivery and consumption dynamics in algal photobioreactors are critical to unravel microalgae's full potential for bioproduct generation and carbon capture from flue gas streams. This study aims to expand our current understanding by cultivating the diatom *Cyclotella* under controlled process conditions of a bubble column photobioreactor and analyzing CO_2 consumption dynamics in real time using results from an online CO_2 sensor connected to the reactor exhaust. Two sets of experiments were conducted: they served to contrast the influence of silicon and nitrate (Si&N colimitation) and Si limitation, and the light availability, respectively. CO_2 consumption was calculated based on the mass balance around the reactor inlet and outlet gas streams. Biomass samples and lipid extracts were analyzed for carbon (C) content to determine biomass-C and lipid-C concentrations. The outlet CO_2 concentrations varied significantly with cultivation time and process conditions. More than 15% to 65% of the CO_2 introduced left the reactor in the exhaust at any instance based on the set CO_2 transfer rates. The highest average daily capturing efficiency was 60%. Nutrient limitation regimes imposed generated unique CO_2 consumption profiles undiscernible by the biomass-C analysis, i.e. unlike Si limitation, N limitation had more immediate detrimental effects on C consumption. Final biomass-C concentration increased with increasing N and light availability, 275 mg/L vs. 336 mg/L, and 270 mg/L vs. 501 mg/L, respectively. Biomass-C based capturing efficiency approximations resulted in 20% to 40% underestimation. Under Si-limited conditions, the higher light intensity increased the final lipid-C to biomass-C ratio by two times (from 20% to 40%) and the final lipid-C concentration and peak productivity by four times (from 56 mg/L to 216 mg/L, from 7 to 30 mg/L-day, respectively). This study demonstrates online exhaust CO_2 concentration-based analysis's unique capabilities for assessing carbon availability and capture, organic-C production, and its diversion to biomass and lipid production.

Key words: Diatom, algae, photobioreactor, carbon dioxide, biomass, lipid

1. Introduction

The physiological response of algae to increased CO_2 levels has been of research interest due to its pertinence for natural and engineered systems. Algae's major role as an atmospheric carbon sink necessitated the study of their growth response to elevating atmospheric CO_2 concentrations (Gao and Campbell, 2014). Several photobioreactor systems have been developed in response to the growing commercial interest in algae-based products (Iglina et al., 2022). The research efforts on productivity maximization frequently involved the study of CO_2 availability enhancement through CO_2 enrichment in the aeration gas streams (Singh and Singh, 2014). Algae's exceptional ability to thrive under high CO_2 concentrations generated the research interest to assess their potential for use as CO_2-capturing agents from postcombustion flue gas streams (Zhao and Su, 2014; Pashchenko, 2022).

A vast number of studies focused on the effects of aeration gas CO_2 partial pressure (pCO_2) on the productivity of photobioreactors. They show that algal growth is possible with pCO_2 ranging from 0.038% to 100% (v/v), but the optimum range is usually below 10% (Zhao and Su, 2014). Furthermore, increasing pCO_2 generates three distinct growth regimes: limited, optimum, and inhibited (Zhao and Su, 2014). Growth inhibition at excessive pCO_2 is explained by pH drop due to elevated carbonic acid concentrations (Hulatt and Thomas, 2011; Rorrer, 2015). Below optimum pH, cells have to divert more of their metabolic energy for internal pH stabilization (Zhao and Su, 2014).

To estimate CO_2 availability in algal photobioreactors, both the transfer rate of CO_2 to the medium and its consumption rate by the algal cells should be considered (Langley et al., 2012; Jones and Harrison, 2014). Equation 1 can be used to determine

* Correspondence: altanozkan@iyte.edu.tr

the CO_2 transfer rate from the aeration gas to the medium,

$$\frac{dC_{CO_2}}{dt} = k_{La} \times \left(C_{CO_2}{}^{*} - C_{CO_2}\right) \quad (1)$$

where C_{CO2} and $C_{CO2}{}^{*}$ are the concentration of CO_2 in the aqueous phase and the concentration that would be attained under equilibrium with pCO_2 of the aeration gas introduced, respectively, in unit of mM, k_La is the mass transfer coefficient of the system, which depends on parameters such as gas flow rate and bubble size along with medium properties (Rorrer, 2015).

During batch photobioreactor cultivation, the CO_2 transfer rate must exceed the highest consumption rate by the algae to avoid limitations (Rorrer, 2015). Thus, the studies that rely solely on pCO_2 to characterize algal productivity kinetics may be misleading, especially when results from different reactors with different gas diffusers and flow rates are compared (Langley et al., 2012; Jones and Harrison, 2014). Indeed, Jones and Harrison reported similar biomass productivities in airlift reactors regardless of the aeration gas pCO_2 as long as CO_2 transfer rates stayed above a certain threshold (Jones and Harrison, 2014). Similarly, Langley et al. reported a plateau in algal biomass production and carbon uptake rates above a pCO_2 value of 0.0012 atm (Langley et al., 2012).

Microalgae's unique high-rate autotrophic growth capabilities motivated the research on their utilization as carbon-capturing agents from industrial flue gas streams (Kumar et al., 2014; Lara-Gil et al., 2016; Thomas et al., 2016; Singh et al., 2019; Iglina et al., 2022;Pashchenko, 2022; Sanaye Mozaffari Sabet and Golzary, 2022). Direct, injection-based, and indirect, chemical adsorbents and absorbents-based methods have been developed for carbon delivery (Thomas et al., 2016). These research efforts showed the direct method's superiority in process economics and the distinct ability of certain species to thrive under the extreme growth conditions generated from direct flue gas injection to the cultivation medium (Thomas et al., 2016; Singh et al., 2019; Iglina et al., 2022). The CO_2 transfer rate also controls the carbon capture efficiency from the injected flue gas streams (Langley et al., 2012). Aside from the high algal growth rate, the establishment of high efficiencies rests on two conditions: the carbon transfer rate to the cultivation media should (i) be kept high to ensure the near complete availability of gaseous CO_2 for fixation and (ii) be close to the consumption rate to ensure near complete utilization of the available CO_2.

The studies reported in the literature on CO_2 availability assessment in algal photobioreactors almost exclusively rely on the influence of the inlet pCO_2; those that assess CO_2 consumption and capture efficiency mostly rely on biomass production and the associated carbon analyses (Leflay et al., 2021; Singh and Singh, 2014). A small number of studies employed online sensors to understand consumption kinetics (Chiu et al., 2008, 2011; Sydney et al., 2010; Li et al., 2011; Ozkan and Rorrer, 2017a, 2017b; Leflay et al., 2021). However, no comprehensive study assesses (i) how the availability and consumption dynamics change throughout the cultivation time under varying nutrient and light availability regimes imposed and (ii) how these consumption dynamics compare to those estimated based on biomass carbon analyses. This study aims to fill this gap in the literature by cultivating the diatom *Cyclotella* under controlled process conditions of a bubble column photobioreactor equipped with an online infrared CO_2 analyzer to monitor exhaust CO_2 concentration in real time. Comparative cultivation experiments were conducted in terms of metabolic productivity controlling process conditions, including initial silicon-to-nitrate ratios and light availability. The results were compared against those obtained with the elemental analysis of biomass to assess conformity; the lipid extracts were also analyzed to estimate the extent of diversion to this industrially relevant metabolite.

2. Materials and methods

2.1. Inocula preparation

Cyclotella sp. starter culture was obtained from the UTEX Algae Culture Collection at the University of Texas at Austin. The inocula used to initiate the photobioreactors were cultivated in Harrison's artificial seawater medium in 500-mL flasks at a temperature of 22 °C and a light intensity of 100 μE/m²-s under 14-h light and 10-h dark cycles. The cultures were manually mixed once every day. Cultures at the log growth stage were first washed with fresh nutrient media following centrifugation at 1000 × *g* for 10 min (IEC CL30, Thermo Electron Corporation) and added to the reactors for inoculation.

2.2. Photobioreactor design

Figure 1 presents the schematic of the bubble-column photobioreactor used for the study. The cultivation vessel was a Pyrex glass cylinder with a diameter of 10 cm and a height of 69 cm. All photobioreactor connections were leak-free, thus enabling the strain's axenic growth. A stainless steel aeration gas sparger (A-228, Western Analytical Products) with a pore size of 2 μm was installed on the bottom plate. Two mass flow controllers (FMA5518ST and FMA5504ST, Omega) mixed CO_2 and air streams and generated gas flow rates and CO_2 concentrations specified in Table 1. An online infrared CO_2 analyzer (Li-820, Li-COR) measured and recorded the CO_2 concentration in the exhaust gas once every minute. Twelve 50 W halogen light bulbs arranged

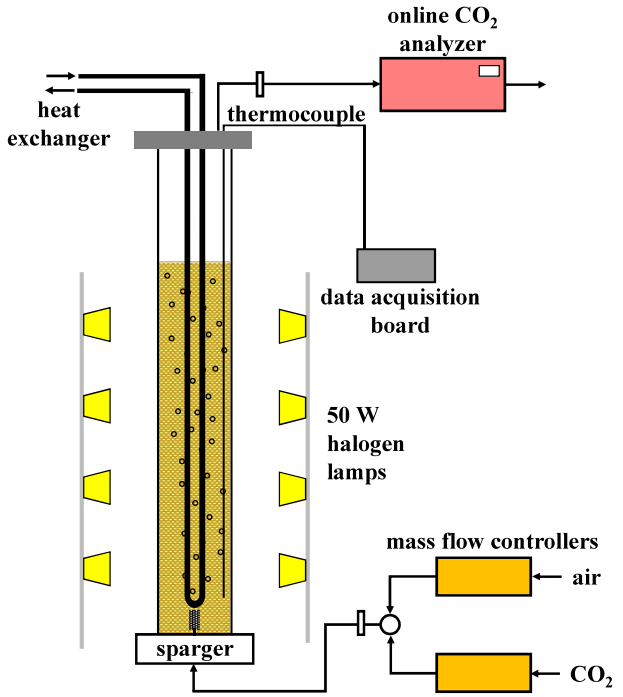

Figure 1. The schematic of the bubble column photobioreactor utilized for the experiments.

in three vertical towers were used as the light source. A dimmer switch was incorporated to adjust the light intensity. A series of measurements were made with a photosynthetically active radiation sensor (190 SL, Li-COR) at the inner surface of the glass cylinder to characterize the relation between the dimmer setting and average incident light intensity as described previously (Ozkan and Rorrer, 2017b). The cultivation temperatures were adjusted to 22 °C by pumping temperature-controlled water through the heat-exchanging coil inserted into the photobioreactor.

2.3 Photobioreactor cultivation experiments

The photobioreactor experiments were designed to study the CO_2 consumption dynamics of the diatom cultures under different process conditions and the correlation of this consumption to biomass and lipid carbon production (Table 1). Two sets of experiments were designed to assay the influence of nutrient limitation and light availability.

2.3.1. First set of photobioreactor cultivation experiments: Runs 1 and 2

The first set consisted of two cultivation experiments under identical process conditions other than the initial dissolved nitrate (N) to silicon (Si) ratio of the cultivation media, as presented in Table 1. The Si dosages allowed the study of the carbon consumption dynamics under first silicon replete and then deplete conditions. The initial dissolved N levels were set (i) to expose the first culture (Run 1) to dissolved N limitation following Si (Si&N co-limitation) and (ii) to grow the second culture (Run 2) under constant N availability (Si limitation). The cultivation continued for about 140 h after dissolved Si depletion to characterize carbon consumption patterns and reveal the differences arising from the nutrient limitation regimes imposed. The prolonged study of this phase was particularly essential as diatoms are known to shift their metabolism towards lipid biosynthesis under Si-limited growth (Mansour et al., 2005). The aeration gas flow rate and pCO_2 were set to 500 mL/min and 2000 ppm, respectively. Each day, three samples were taken from the suspensions: one just before the light period,

Table 1. Photobioreactor cultivation process conditions

Process parameter	Run 1	Run 2	Run 3	Run 4	Units
Initial culture volume	4.5	4.5	4.5	4.5	L
Cultivation temperature	22	22	22	22	°C
Aeration gas flow rate	500	500	600	600	mL/min
CO_2 partial pressure aeration gas	2000	2000	3000	3000	ppm
k_La (O_2)	43	43	43	43	h^{-1}
Initial [HCO_3^-]	11.8	11.8	16.8	16.8	mM
Initial cell number density	2.0×10^5	2.0×10^5	1.0×10^5	1.0×10^5	cells/mL
Initial silicon concentration	0.80	0.80	1.80	1.80	mM
Initial nitrate concentration	1.1	5.3	7.0	7.0	mM
Average incident light intensity	300	300	20	30/100	$\mu E/m^2$-sec
Light:dark period	14:10	14:10	14:10	14:10	hour/hour

k_La (O_2): volumetric mass transfer coefficient for O_2 (g)

one at the middle of the light period, and one just before the dark period. The cell number densities were measured with a cell counter (Model Z2, Beckman Coulter Counter) at a minimum threshold of 6 μm in triplicates. Dissolved Si and N concentrations were measured with spectrophotometric methods as described previously (Ozkan and Rorrer, 2017a). Following the onset of the dissolved Si depletion, additional samples were taken every 48 h to assess total biomass dry weight (Zhu and Lee, 1997). These samples were centrifuged at 1000 × *g* for 10 min and washed with 0.599 M NaCl solution twice. The centrifuge pellets were dried in an 80 °C oven for 18 h. The dried samples were weighed using an analytical scale.

2.3.2. Second set of photobioreactor cultivation experiments: Runs 3 and 4

The second set consisted of two cultivation experiments that only differed by the incident light intensities, as presented in Table 1. Run 3 had an average incident light intensity of 20 μE/m^2-s. During Run 4, cells were cultivated at an average incident light intensity of 30 μE/m^2-s until the cell number density plateaued, and after that (after the 125th h), the light intensity was increased to 100 μE/m^2-s. The aeration rate and pCO_2 were 600 mL/min and 3000 ppm, respectively. The initial dissolved Si concentrations were 1.80 mM. The cultivation continued for at least 8 days after dissolved Si depletion to assess its influence on inorganic carbon consumption and the diversion of the produced organic carbon to biomass and lipid synthesis. The initial nitrate concentrations were set to ensure constant N availability during the whole growth period.

2.4. Lipid extraction and quantification

A modified Folch method was utilized to extract lipids from the dried biomass samples (Ways and Hanahan, 1964). The samples were first crushed into powder with mortar and pestle, and then 5 mL of 2:1 (v:v) $CHCl_3$:MeOH solution was added. The lipids were extracted under constant shaking at 180 RPM (Lab-Line Orbit Environ Shaker, Lab-Line Instruments). After 12 h of extraction, the samples were left undisturbed for 30 min for the solids to settle. The solvent layer on top was decanted. The extraction process was repeated twice more using 2.5 mL of the same binary solvent mixture to extract any remaining lipids. The extractants were combined and washed first with 5 mL of 0.88% (w/v) KCl and then with 5 mL of 1:1 (v:v) MeOH:H_2O. After each wash, the solvents were separated with centrifugation at 750 × *g* for 10 min, and the upper phases containing the lipids were pipetted. A previously published method was used to quantify the mass of the lipid extracts (Hellebust JA, 1978; Ryu and Rorrer, 2010; Jeffryes et al., 2013).

2.5. Elemental analysis of biomass and lipid samples

Dried biomass samples were analyzed with an organic elemental analyzer (Flash 2000, Thermo Scientific) to determine the carbon contents. Samples with masses ranging from 2 to 6 mg were weighed in tin capsules (240-064-25, CE Elantech Inc.) using a precision scale (XS105, Mettler Toledo). The analyzer's furnace temperature was 950 °C, and the oven temperature for the thermal conductivity detector column was 65 °C. The carrier and reference helium flow rates were set to 140 mL/min and 100 mL/min, respectively. The oxygen flow rate was 250 mL/min. Lipids extracted were dried under constant nitrogen flow and analyzed for carbon content with the same method.

2.6. Data analysis

The cell number density, biomass carbon, and lipid carbon vs. cultivation time profiles were sigmoidal. Thus, the logistic model was fitted to the results with nonlinear, least squares regression using the Marquardt method on Statgraphics Centurion Software to assess the cultivation condition's influence on productivity characteristics (Shirazian et al., 2022). The model used is defined as:

$$X_{P-i}(t) = \frac{X_{0,P-i} e^{k_{P-i}(t)}}{1 + \frac{X_{0,P-i}}{X_{f,P-i}}(e^{k_{P-i}(t)} - 1)} \quad (2)$$

where X_{P-i} is the product concentration at time t, i.e. cell number density (cells/mL), biomass carbon or lipid carbon concentrations (mg/L), $X_{0,P-i}$ and $X_{f,P-i}$ are the initial and final product concentrations (cells/mL for cell or mg/L for biomass or lipid carbon), respectively, k_{P-i} is the logistic model rate constant (h^{-1}). The peak productivities were quantified by

$$R_{P-i} = \frac{k_{P-i} X_{f,P-i}}{4} \quad (3)$$

where R_{P-i} is the peak productivity in cells/mL-day for cell and in mg/L-day for biomass and lipid carbon productions. These quantified logistic model parameters ($X_{f,P-i}$, k_{P-i}, and R_{P-i}) characterized the productivities obtained at each run for each product, which in turn assisted with the comparison of the results at a higher accuracy.

3. Results and discussion

3.1. Cell production and nutrient consumption

Figure 2 compares the cell number density, dissolved silicon (Si) and nitrate (N) concentrations vs. cultivation time profiles during photobioreactor cultivation under varying nutrient and light availability regimes. Si availability controlled the cell division and the final cell number densities, i.e. 48 h after dissolved Si depletion, cell number densities reached a plateau. This dependence

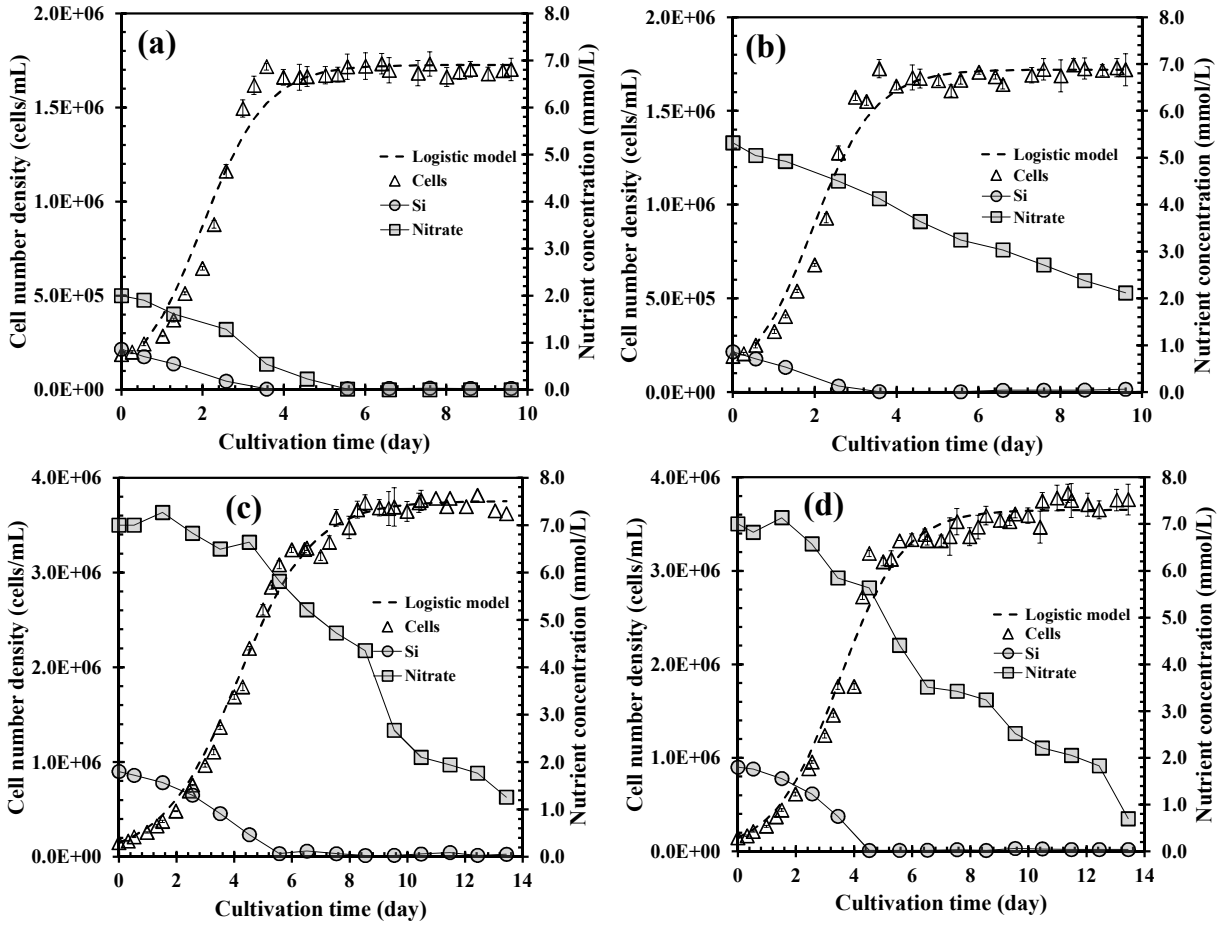

Figure 2. Comparison of the cell number density, dissolved silicon, and nitrate concentration vs. cultivation time profiles during photobioreactor cultivation of the diatom *Cyclotella* sp. (a) Run 1 (Si&N colimitation), (b) Run 2 (Si limitation), (c) Run 3 ($I_{0\text{-}mean}$=20 μE/m^2-s), and (d) Run 4 ($I_{0\text{-}mean\text{-}log}$ =30 μE/m^2-s, $I_{0\text{-}mean\text{-}st}$=100 μE/m^2-s). Each data point represents the mean ± 1.0 S.E. of at least triplicate measurements.

is in accordance with diatoms' characteristic ability to intake dissolved silicon and synthesize silica-based cell walls called frustules (Lopez et al., 2005). The cells maintained their N consumption during the stationary growth phases, as evidenced by the dissolved N profiles obtained with Runs 2-4. Algae, including species belonging to the *Cyclotella* genus, usually follow Monod kinetics with respect to nitrate and have half-saturation constants (K_s) in the micromolar range (Eppley et al., 1969). Thus, it is safe to assume that these three runs maintained N-replete growth conditions at all times during cultivation. In the case of the first run, the cells depleted N about 48 h after Si depletion.

Figure 3a compares the measured cell number density results with those predicted by the logistic model (Equation 2). It shows that the measured values fall within 20% of model predictions. The final cell number densities ($X_{sf\text{-}cells}$) were indifferent to nitrate (N) limitation: Si and N colimited and Si-limited growth regimes generated $X_{sf\text{-}cells}$ of about 1.7 × 10^6 cells/mL. In parallel, light availability experiments resulted in $X_{sf\text{-}cells}$ of about 3.7 × 10^6 cells/mL. The initial Si dosage seems to be the most critical factor for the extent of cell production, as indicated by the similar final cell yield on silicon ($Y_{sf\text{-}cells/Si}$) values obtained across all the runs. Indeed, diatom cell walls are known for having well-defined silica contents (Hildebrand et al., 2012). Runs 3&4 resulted in lower cell production rate constants ($k_{P,cells}$) than the first two runs. This was likely due to growth under lower light availability. Indeed, Ozkan and Rorrer reported saturation-type kinetics between light availability and cell production rate with the current strain (Ozkan and Rorrer, 2017b). Furthermore, $Y_{sf\text{-}cells/Si}$ values were similar regardless of the variations in the incident light intensity (Ozkan and Rorrer, 2017b). Diatoms' well-defined Si requirement for cell wall formation dictated the extent of cell production, while other process parameters, such as the light intensity, controlled the associated rate.

3.2. Photobioreactor exhaust CO_2 concentration

Figures 4a and 4b present the comparison of the diurnal variation in the CO_2 concentration measured at the photobioreactor exhaust. The inlet CO_2 concentrations were fixed at 2000 ppm and 3000 ppm for the 1st and the 2nd set of experiments, respectively. The cells oscillated between acting as CO_2 sinks or sources in response to the imposed light/dark (14 h/10 h) periodicity. They consumed dissolved CO_2 during the light periods through photosynthesis. The deficit created in the aqueous phase was replenished with CO_2 transferred from the aeration gas and also with CO_2 generated from bicarbonate dehydration (Kong et al., 2021). Diatoms can also consume bicarbonate to varying degrees through deliberate enzymatic conversion to CO_2 at the cell surface or through active transport (Matsuda et al., 2017). Following the transition to the dark phase, photosynthesis stopped, and the deficiency in the total dissolved inorganic carbon (CO_2(aq) and HCO_3^-) got replenished by CO_2 transferred from the aeration gas CO_2 until equilibrium (pCO_2-*inlet*=pCO_2-*exhaust*) was established. During dark periods, the cells only respired and released extra CO_2 to the cultivation medium.

Outlet pCO_2 varied significantly during the 14-h light periods. In this regard, the results point to the need for improvement in reactor geometry or configurations for the constant maintenance of a set minimum exhaust gas pCO_2. The lowest pCO_2 measured in the exhaust

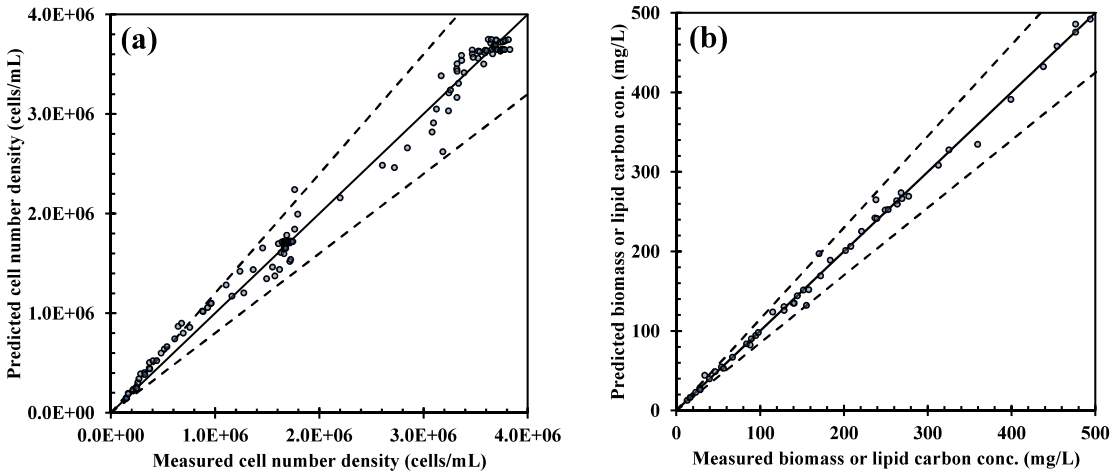

Figure 3. Comparison of measured results and logistic model predictions (Equation 2) for (a) cell number density and (b) biomass or lipid carbon concentrations. The dashed line for figures a and b present ±20% and ±15% deviation from model predictions, respectively.

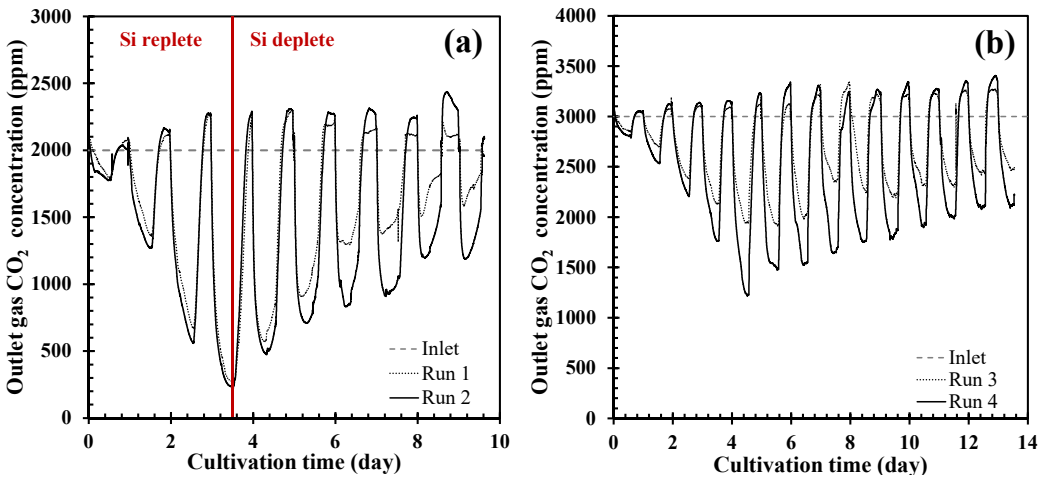

Figure 4. Comparison of diurnal variation in the outlet CO_2 concentration during photobioreactor cultivation of the diatom *Cyclotella* sp. (a) Run 1 (Si&N colimitation) vs. Run 2 (Si limitation), and (b) Run 3 ($I_{0\text{-}mean}$=20 µE/m²-s) vs. Run 4 ($I_{0\text{-}mean\text{-}log}$ =30 µE/m²-s, $I_{0\text{-}mean\text{-}st}$=100 µE/m²-s).

was about 300 ppm for Runs 1&2, 1226 ppm for Run 3, and 1934 ppm for Run 4. This points to CO_2-replete growth conditions and means that at any moment during cultivation, more than 15%, 40%, and 65% of the CO_2 introduced to the photobioreactor left the system in the exhaust with Runs 1&2, 3, and 4, respectively.

The outlet CO_2 concentration profiles reflect nutrient and light availability's influence on diatom metabolism. For instance, they overlapped to a large extent for Runs 1&2 until the dissolved nitrate exhaustion, which happened sometime between the 110th and 134th h of cultivation. Following this point, the detrimental effects of nitrogen limitation can be clearly discerned through the higher exhaust CO_2 concentrations obtained during light periods with Run 1. This capturing efficiency reduction can be attributed to chlorophyll degradation and photosystem inhibition observed with algae under nitrogen-limited growth conditions (Fan et al., 2014). In this regard, the results highlight the unique productivity advantage the Si limitation offers in manipulating metabolic activity towards the production of target products such as lipids (Martin-Jezequel et al., 2000). This is mainly due to the absence of Si's direct involvement with the diatom energy metabolism (Hildebrand et al., 2012). Comparison of exhaust CO_2 profiles from Runs 3&4 point to an increased CO_2 consumption at higher incident light intensity as this was the only process parameter that was varied between the experiments (Table 1). Constant monitoring of exhaust CO_2 concentration enabled the apprehension of the influence process conditions had on diatoms' carbon consumption dynamics.

3.3. Cumulative CO_2 consumption, and biomass and lipid carbon production

The cumulative CO_2 consumption of the cultures was quantified based on mass balance around the photobioreactor. The difference between the inlet and the outlet streams vs. cultivation time profiles were numerically integrated according to:

$$X_C(t) = \frac{v_0\, P}{RT\, V_L} \int_0^t \left(Y_{CO_2,in} - Y_{CO_2,out}\right) dt \tag{4}$$

where X_C is the algal CO_2 consumption in mM, v_0 is the volumetric gas flow rate in L/h, $Y_{CO2,in}$ and $Y_{CO2,out}$ are the mole fraction of CO_2 in the inlet and outlet gas streams, respectively, V_L is the culture volume in L, R is the universal gas constant in L/atm-mol, and T is the cultivation temperature in K.

The cumulative CO_2 consumption vs. cultivation time profiles had a saw-tooth pattern, i.e. the light and dark periods were marked by positive and negative slopes, respectively (Figure 5). This resulted from the aforementioned oscillations observed in the exhaust CO_2 concentrations (Figure 4). Through respiration, the cells released up to 5% of their cumulative carbon consumption during the 10-h daily night-time periods. The average daily losses were less than 2% for all the runs. The night-time respiratory activity was higher during the log than the stationary phases. This was likely due to higher log-phase night-time metabolic activity, as also evidenced by the cell number density increases recorded during these periods. These results agree with previous research on night-time biomass losses with algae both in terms of the fraction of losses recorded and its reduction with the transition from log to stationary phase (Edmundson and Huesemann, 2015).

The cumulative CO_2 consumption reached a plateau at the end of the first run, while all the rest maintained an overall increasing trend throughout the whole cultivation period (Figure 5). As already discussed, the stationary phase reached with nitrogen limitation likely resulted from its destructive influence on the photosystem. On the contrary, a net increase in cumulative CO_2 consumption could be observed even 200 h after dissolved silicon depletion and 150 h after reaching stationary cell number density corresponding to the cultivation time after the 215th h in Figure 5b. This difference between the influences of nutrient limitations on diatom physiology resulted in an additional final CO_2 consumption of about 130 mg/L with Run 2. The general trend of CO_2 consumption vs. cultivation time profiles for the 2nd set of experiments could be approximated with linear lines, whose slopes increased with increasing light availability (Run 3 vs. Run 4). The influence of light limitation on CO_2 consumption rate and final consumption concentration are clearly demonstrated, i.e. with increasing light availability, CO_2 consumption of the strain increased from 500 mg/L to about 850 mg/L at the end of the 350th h (Figures 5c and 5d).

Biomass-C concentrations reached the stationary phase with all the runs at least 48 h before the end of the cultivation period. In this regard, for Runs 2-4, they contradicted the cumulative carbon consumption profiles, which steadily increased throughout the whole growth period and exceeded the biomass-C concentrations (Figures 5b–5d). This gap can be explained by the deliberate release of organic carbon by the cells and also by cell lysis resulting from the hydrodynamic shear force the cultures experienced during growth. Diatoms are known to biosynthesize extracellular polymeric substances (EPS) for various functions like motility, adhesion, and protection from adverse environmental changes (Hoagland et al., 1993; Shniukova and Zolotareva, 2015). In particular, the genus *Cyclotella* produces pure chitin nanofibers, accounting for up to 30% of the dry biomass, and extrudes them to the cell exterior through

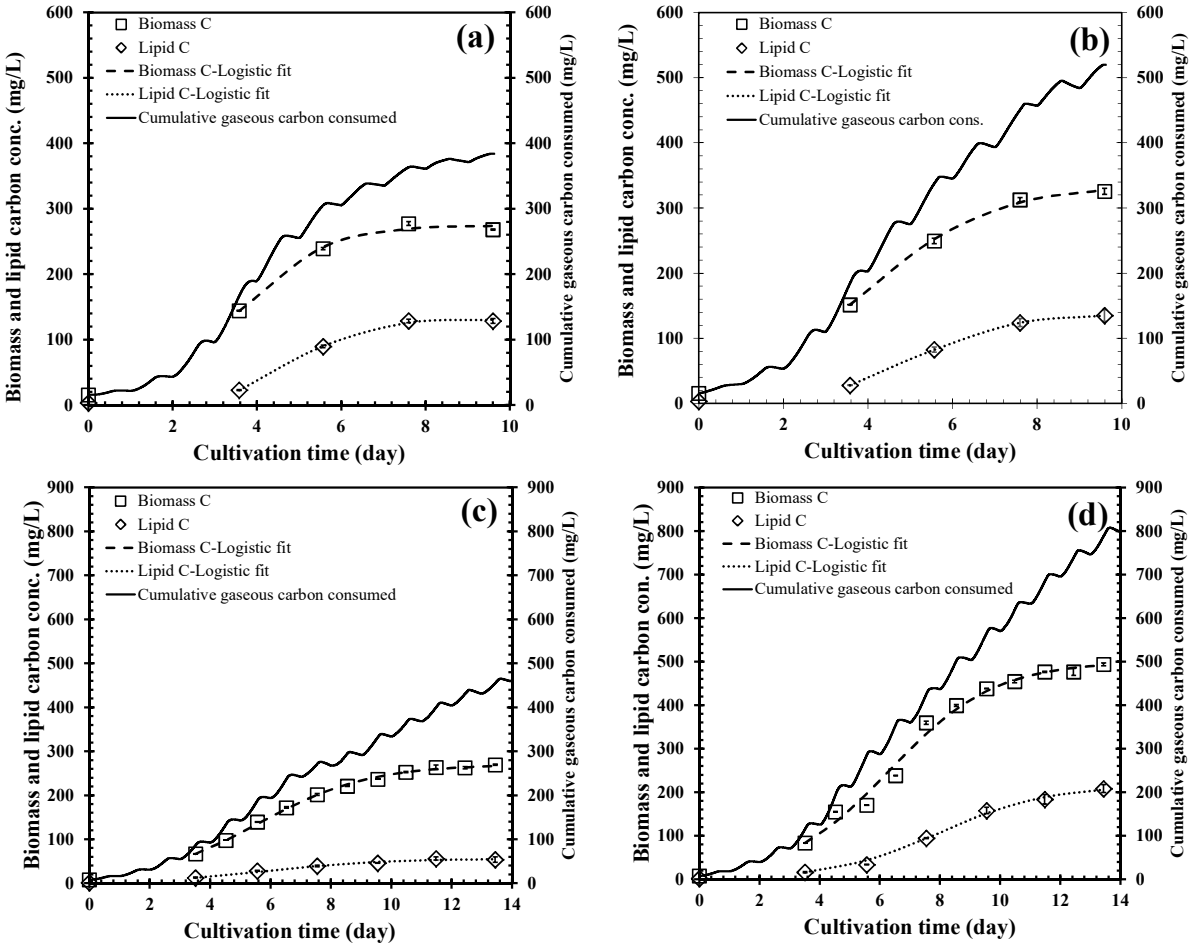

Figure 5. Comparison of cumulative gaseous CO_2 consumption (calculated according to Equation 4), and biomass and lipid carbon concentrations during photobioreactor cultivation of the diatom *Cyclotella* sp. (a) Run 1 (Si&N co-limitation), (b) Run 2 (Si limitation), (c) Run 3 ($I_{0\text{-}mean}$=20 µE/m^2-s), and (d) Run 4 ($I_{0\text{-}mean\text{-}log}$ =30 µE/m^2-s, $I_{0\text{-}mean\text{-}st}$=100 µE/m^2-s). Each data point represents the mean ± 1.0 S.E. of at least triplicate measurements.

specialized ports (Ozkan and Rorrer, 2017b). These fibers can get dislodged from the cells due to exposure to hydrodynamic shear force during growth (LeDuff and Rorrer, 2019). In the current work, the centrifuge speed selected for biomass harvesting (1000 × *g*) was highly effective in capturing the diatom cells but likely failed to maintain the same effectiveness for capturing the free nanofibers, which were harvested effectively at 16,000 × *g* in previous work (Ozkan and Rorrer, 2017b, 2017c). Lysis is another effect the hydrodynamic shear force has on the cells that reduces the effectiveness of centrifugal biomass harvesting. This mainly results from the leakage of the water-soluble organic cell constituents into the cultivation media (Zhang et al., 2016; Wang and Lan, 2018).

Figure 3b compares the biomass and lipid carbon concentrations measured experimentally with those predicted by the logistic model (Equation 2). It indicates that the model predicts the measured results within 15%. Final biomass-C concentrations ($X_{,f\text{-}biomass\ C}$) increased with increasing nitrogen (N) and light availability, 275 ± 6 mg/L vs. 336 ± 5 mg/L, and 270 ± 2 mg/L vs. 501 ± 12 mg/L, respectively (Table 2). As opposed to the cell yield on silicon ($Y_{f\text{-}cell/Si}$) that was constant across the runs, the biomass carbon yield on Si ($Y_{biomass\text{-}C/Si}$) varied significantly. Lipid-C concentrations reached a plateau within the cultivation periods. The final lipid-C concentration ($X_{,f\text{-}lipid\ C}$) was independent of nitrogen availability. However, the final concentration was reached sooner at under N-limited growth (Run 1), as also indicated by the higher rate constant ($k_{P,\,lipid\,C}$). The results clearly show the influence of light availability on lipid production (Run 3 vs. Run 4). At higher light availability (Run 4), the final lipid-C concentration and the peak lipid-C productivity ($R_{P\text{-}lipid\,C}$) were about four times those obtained under lower light availability (Run 3). Runs 3&4

Table 2. Productivity parameters and rate constants for photobioreactor cultivation experiments. All errors are ±1.0 standard error (S.E.)

Parameter & units	**Run 1**	**Run 2**	**Run 3**	**Run 4**
$X_{,f\text{-}cells}$ (cells/mL)	$1.73{\cdot}10^{6} \pm 2.5{\cdot}10^{4}$	$1.72{\cdot}10^{6} \pm 2.4{\cdot}10^{4}$	$3.75{\cdot}10^{6} \pm 2.8{\cdot}10^{4}$	$3.65{\cdot}10^{6} \pm 4.0{\cdot}10^{4}$
$k_{P,cells}$ (h^{-1})	$5.25{\cdot}10^{-2} \pm 2.4{\cdot}10^{-3}$	$5.40{\cdot}10^{-2} \pm 2.5{\cdot}10^{-3}$	$3.22{\cdot}10^{-2} \pm 4{\cdot}10^{-4}$	$3.77{\cdot}10^{-2} \pm 8{\cdot}10^{-4}$
$R_{P\text{-}cells}$ (cells/mL-day)	$5.45{\cdot}10^{5} \pm 2.6{\cdot}10^{4}$	$5.57{\cdot}10^{5} \pm 2.7{\cdot}10^{4}$	$6.22{\cdot}10^{5} \pm 9.4{\cdot}10^{3}$	$8.53{\cdot}10^{5} \pm 4.0{\cdot}10^{4}$
$X_{,f\text{-}biomass\ C}$ (mg/L)	275 ± 6	336 ± 5	270 ± 2	501 ± 12
$k_{P,biomass\ C}$ (h^{-1})	$3.94{\cdot}10^{-2} \pm 6.4{\cdot}10^{-3}$	$2.72{\cdot}10^{-2} \pm 1.6{\cdot}10^{-3}$	$2.25{\cdot}10^{-2} \pm 5{\cdot}10^{-4}$	$2.38{\cdot}10^{-2} \pm 1.1{\cdot}10^{-3}$
$R_{P\text{-}biomass\ C}$ (mg/L-day)	65 ± 11	55 ± 3	36 ± 1	72 ± 4
$X_{,f\text{-}lipid\ C}$ (mg/L)	131 ± 2	137 ± 9	56 ± 2	216 ± 8
$k_{P,\ lipid\ C}$ (h^{-1})	$4.90{\cdot}10^{-2} \pm 2.1{\cdot}10^{-3}$	$3.71{\cdot}10^{-2} \pm 5.7{\cdot}10^{-3}$	$2.20{\cdot}10^{-2} \pm 2.1{\cdot}10^{-3}$	$2.32{\cdot}10^{-2} \pm 1.0\ 10^{-3}$
$R_{P\text{-}lipid\ C}$ (mg/L-day)	39 ± 2	30 ± 5	7 ± 1	30 ± 2
$Y_{f\text{-}cell/Si}$ (10^{9} cells/mM Si)	2.16 ± 0.03	2.15 ± 0.03	2.08 ± 0.02	2.03 ± 0.02
$Y_{f\text{-}biomass\text{-}C/Si}$ (mg /mM Si)	344 ± 8	420 ± 6	150 ± 1	278 ± 7

resulted in similar biomass-C and lipid-C production rate constants, demonstrating their simultaneous arrival to the stationary phase. There were systematic differences between the outcomes from the inlet vs. outlet analysis and the elemental analysis-based measurements. They revealed the distinct influence each nutrient limitation had on carbon fixation and accumulation of nonharvestable (with centrifugation at 1000 × *g*) organic carbon-containing metabolites in the aqueous medium, even at fixed biomass carbon concentration.

3.4. Average daily CO_2 capture and organic carbon diversion to biomass and lipid

Average daily CO_2 capturing efficiencies were quantified to assess the extent of CO_2 capture from the aeration gas streams. It was defined as the ratio of the daily CO_2 consumption by the culture (calculated according to Equation 4) to the CO_2 delivered with the aeration gas during the same period. Capturing efficiencies changed drastically with both cultivation time and process conditions. The efficiencies of Runs 1&2 peaked during the first 100 h of growth and reached a maximum value of up to 60% at an inlet pCO_2 of 2000 ppm (Figures 6a and 6b). They decreased sharply after the nutrient limitation and ended at a value below 5% and 20% under Si&N colimited and Si-limited growth conditions, respectively. The second set demonstrates improved light availability's beneficial effects on capturing efficiencies. In parallel to the results from the 1st set, the capturing efficiency reached the highest level at the late log phase at about the 120th h but maintained a more consistent level after Si depletion (Figures 6c and 6d). In this regard, the growth phases maximizing CO_2 capture and lipid production did not overlap. Comparison of the results from both groups points out to the critical role inlet pCO_2 and aeration gas flow rate (v_0) play in establishing high capturing efficiencies: while Runs 1, 2, and 4 had similar ranges of daily CO_2 consumption (as shown in cumulative C consumption profiles in Figures 5a, 5b, and 5d), the average daily capturing efficiencies of the 4th run were significantly lower at both growth stages (Figure 6d).

Figure 6 compares the carbon concentrations determined based on elemental analysis of the dry biomass samples and infrared analysis of the exhaust stream - biomass carbon concentration (measured)/ gaseous CO_2 captured (calculated according to Equation 4). This analysis allowed the estimation of the extent of the nonharvestable (with centrifugation at 1000 × *g*) organic carbon biosynthesized by the cells and released to the cultivation media. This ratio varied from about 0.6 to 0.8 with cultivation time and variations in process conditions, indicating that carbon capturing efficiencies estimated solely using biomass carbon content may lead to significant underestimation. The ratio of nonharvestable organic carbon increased as the culture transitioned from

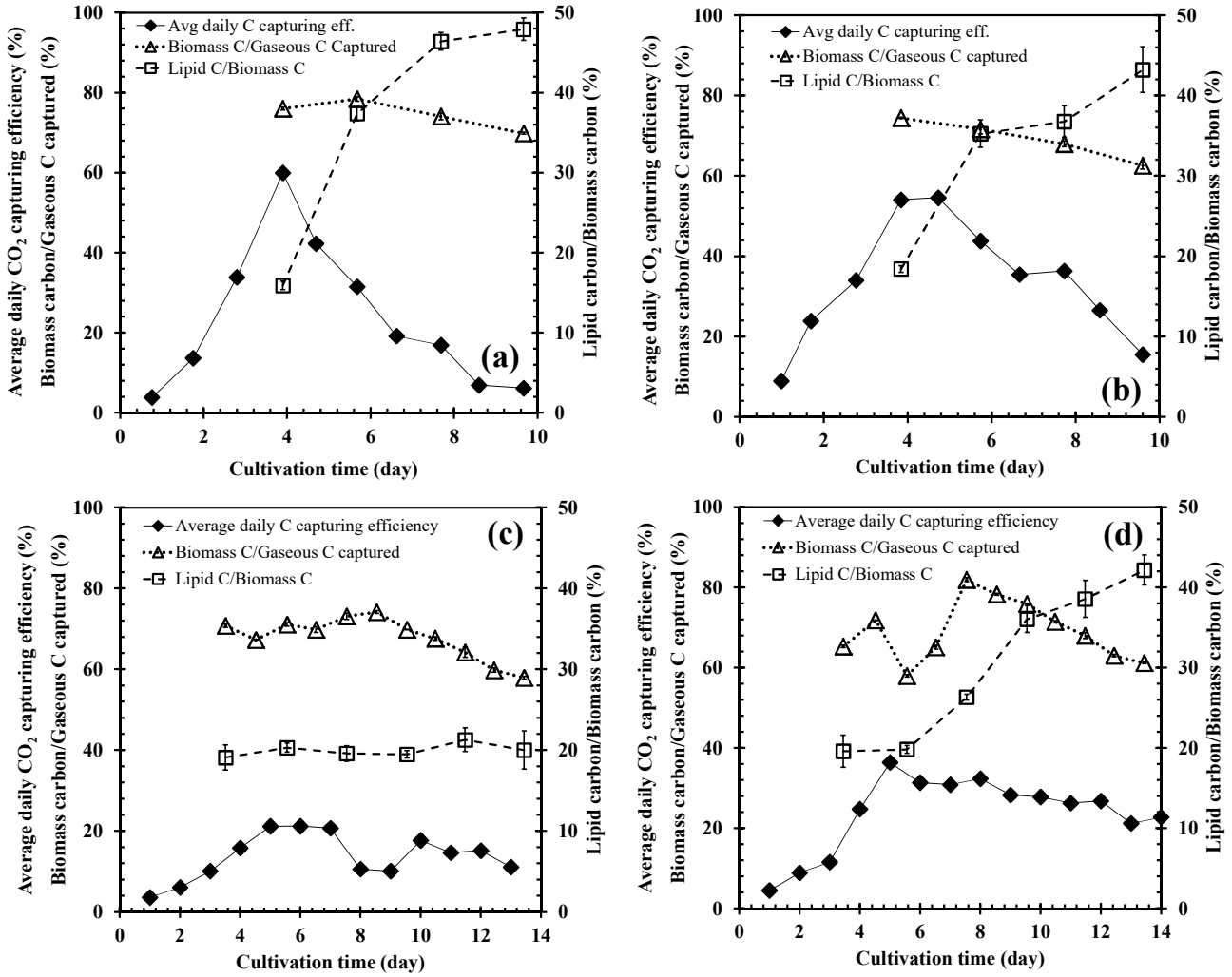

Figure 6. Comparison of the average daily CO_2 capturing efficiency, the ratio of biomass carbon concentration (measured experimentally)/gaseous CO_2 captured (calculated according to Equation 4), and the ratio of lipid carbon/biomass carbon during photobioreactor cultivation of the diatom *Cyclotella* sp. (a) Run 1 (Si&N co-limitation), (b) Run 2 (Si limitation), (c) Run 3 ($I_{0\text{-}mean}$=20 μE/m^2-s), and (d) Run 4 ($I_{0\text{-}mean\text{-}log}$ =30 μE/m^2-s, $I_{0\text{-}mean\text{-}st}$ =100 μE/m^2-s). Each data point represents the mean±1.0 S.E. of at least triplicate measurements.

the log to the stationary phase, which can be explained by the increased diversion of the organic carbon produced to chitin nanofiber and EPS production pathways under such conditions (Hoagland et al., 1993; LeDuff and Rorrer, 2019).

Lipid carbon concentrations were compared against biomass carbon concentrations to estimate the extent of organic carbon diversion to lipids (Figure 6). Runs 2 and 4 clearly demonstrate the favorable influence Si depletion has on lipid production: the lipid carbon ratio in biomass increased from an initial value ranging from 15% to 20% to above 40% following the onset of dissolved silicon depletion (Figures 6b and 6d). With Si&N colimitation, the lipid carbon content plateaued at a similar final level but reached there 48 h prior compared to the Si-limited growth regime. Runs 3&4 clearly show the influence of light availability on biomass lipid content. Under lower light intensity (Run 3), the lipid ratio was constant at 20% regardless of nutrient availability or cultivation time (Figure 6c). Thus, it can be concluded that the increased light intensity not only doubled the carbon consumption and production of biomass carbon but also increased the ratio of carbon diverted to lipid synthesis. Cultivation time and process conditions controlled the extent of carbon capture from the aeration stream and the diversion ratio of the generated organic carbon pool to harvestable (with centrifugation at 1000 × *g*) metabolites and lipids. At the end of the cultivation periods, about 20% to 40% of the carbon fixed (calculated using Equation 4) was not accounted for based on elemental biomass analysis.

4. Conclusion

The CO_2 consumption dynamics as well as cell, biomass and lipid carbon productivities of the diatom *Cyclotella* were studied under different nutrient and light availability regimes. For this, the diatom was cultivated under controlled process conditions of a bubble column photobioreactor instrumented with an infrared analyzer at the gas exhaust for online CO_2 concentration analysis. This is one of the few studies that assessed the exhaust CO_2 concentration continuously throughout the whole cultivation period and the only study that compared the calculated CO_2 consumption dynamics with the elemental analysis-based biomass and lipid carbon production profiles. The following conclusions can be drawn:

- The diatom cells had well-defined silicon contents, resulting in similar cell yields on silicon across all the runs.
- The exhaust pCO_2 varied significantly with cultivation time, nutrient limitation, and light availability. More than 15% to 65% of the CO_2 introduced left the system in the exhaust at any point during cultivation. The highest average daily CO_2 capturing efficiency was around 60%.
- The cells kept acting as CO_2 sinks under silicon (Si) limitation until the end of the cultivation periods, but combined with dissolved nitrate (N) exhaustion, CO_2 consumption halted within 48 h. Biomass-C vs. cultivation time profiles plateaued 48 h before the end of the growth periods and contradicted the CO_2 consumption profiles. Elemental analysis of the biomass could not account for up to 40% of the CO_2 consumed and pointed to nonharvestable extracellular polymeric substance accumulation in the aqueous phase with cultivation time.
- Both nutrient limitation regimes resulted in a lipid-C concentration of around 110 mg/L and biomass lipid-C content of about 45%. Colimitation increased the rate of lipid accumulation.
- Increased light availability increased the ratio of gaseous CO_2 captured, final biomass C concentration, and the ratio of C diverted to lipid biosynthesis, from about 20% to 40%.
- Future experiments should assess the influence of reactor geometries on the carbon-capturing efficiencies and incorporate species, such as *Chlorella vulgaris*, that show high promise for CO_2 capture from postcombustion flue gas streams.

Nomenclature

C_{CO2} dissolved CO_2 concentration in the aqueous phase (mM)

C_{CO2}^* dissolved CO_2 concentration in the aqueous phase in equilibrium with the aeration gas pCO_2 (mM)

k_La mass transfer coefficient in culture medium (h^{-1})

$k_{P\text{-}i}$ logistic model rate constant for product *i*, with *i*=cell number density, biomass carbon or lipid carbon concentrations (h^{-1})

$I_{0\text{-}mean}$ average incident light delivered to the inner surface of the cultivation vessel (μmol/m^2-s)

P aeration gas pressure (atm)

pCO_2 aeration gas CO_2 partial pressure (ppm or atm)

R universal gas constant (L/atm-mol)

$R_{P\text{-}i}$ peak productivity of product i, *i*=cell number density (cells/mL-day), biomass carbon or lipid carbon concentrations (mg/L-day)

t cultivation time (h)

T cultivation temperature (K)

v_0 volumetric gas flow rate (L/h)

V_L diatom suspension volume (L)

$X_{P\text{-}i}$ product *i* concentration in diatom suspension, with *i*=cell number density (cells/mL), biomass carbon or lipid carbon concentrations (mg/L)

$X_{0,P\text{-}i}$ product concentration at the start of the cultivation, with *i*=cell number density (cells/mL), biomass carbon or lipid carbon concentrations (mg/L)

$X_{f,P\text{-}i}$ product concentration at the end of the cultivation period, with *i*=cell number density (cells/mL), biomass carbon or lipid carbon concentrations (mg/L)

Xc algal CO_2 consumption calculated based on inlet aeration gas and exhaust gas CO_2 concentration difference according to Equation 4 (mM)

$Y_{CO2,in}$ mole fraction of CO_2 in the inlet gas stream (mole/mole)

$Y_{CO2,out}$ mole fraction of CO_2 in the exhaust gas stream (mole/mole)

$Y_{f\text{-}biomass\text{-}C/Si}$ final yield of biomass carbon on silicon (mg/mM Si)

$Y_{f\text{-}cell/Si}$ final yield of cell on silicon (10^9 cells/mM Si)

Subscripts

biomass-C refers to biomass carbon concentration determined based on elemental analysis of dry biomass samples (mg/L)

lipid-C refers to lipid carbon concentration determined based on elemental analysis of lipids extracted from biomass samples (mg/L)

log refers to the log phase of growth

st refers to the stationary phase of growth

Acknowledgments

This work was supported by the US National Science Foundation (NSF), Emerging Frontiers for Research and Innovation program (EFRI), under award number 1240488.

References

Chiu SY, Kao CY, Chen CH, Kuan TC, Ong SC et al. (2008). Reduction of CO_2 by a high-density culture of *Chlorella* sp. in a semicontinuous photobioreactor. Bioresource Technology 99 (9): 3389–3396. https://doi.org/10.1016/j.biortech.2007.08.013

Chiu SY, Kao CY, Huang TT, Lin CJ, Ong SC et al. (2011). Microalgal biomass production and on-site bioremediation of carbon dioxide, nitrogen oxide and sulfur dioxide from flue gas using *Chlorella* sp. cultures. Bioresource Technology 102 (19): 9135–9142. https://doi.org/10.1016/j.biortech.2011.06.091

Edmundson SJ, Huesemann MH (2015). The dark side of algae cultivation: Characterizing night biomass loss in three photosynthetic algae, *Chlorella sorokiniana*, *Nannochloropsis salina* and *Picochlorum* sp. Algal Research 12: 470–476.

Eppley RW, Rogers JN, McCarthy JJ (1969). Half-saturation constants for uptake of nitrate and ammonium by marine phytoplankton. Limnology and Oceanography 14 (6): 912–920.

Fan J, Cui Y, Wan M, Wang W, Li Y (2014). Lipid accumulation and biosynthesis genes response of the oleaginous *Chlorella pyrenoidosa* under three nutrition stressors. Biotechnology for Biofuels 7 (1): 1–14.

Gao K, Campbell DA (2014). Photophysiological responses of marine diatoms to elevated CO_2 and decreased pH: A review. Functional Plant Biology 41 (5): 449–459.

Hellebust JA, Craigie JSC (1978). Handbook of Phycological Methods Physiological and Biochemical Methods. Cambridge University Press.

Hildebrand M, Davis AK, Smith SR, Traller JC, Abbriano R (2012). The place of diatoms in the biofuels industry. Biofuels 3 (2): 221–240.

Hoagland KD, Rosowski JR, Gretz MR, Roemer SC (1993). Diatom extracellular polymeric substances: Function, fine structure, chemistry, and physiology. Journal of Phycology 29: 537–566.

Hulatt CJ, Thomas DN (2011). Productivity, carbon dioxide uptake and net energy return of microalgal bubble column photobioreactors. Bioresource Technology 102 (10): 5775–5787.

Iglina T, Iglin P, Pashchenko D (2022). Industrial CO_2 Capture by Algae: A Review and Recent Advances. Sustainability, 14 (7): 3801. https://doi.org/10.3390/su14073801

Jeffryes C, Rosenberger J, Rorrer GL (2013). Fed-batch cultivation and bioprocess modeling of *Cyclotella* sp. for enhanced fatty acid production by controlled silicon limitation. Algal Research 2 (1): 16–27.

Jones SMJ, Harrison STL. (2014). Aeration energy requirements for lipid production by *Scenedesmus* sp. in airlift bioreactors. Algal Research 5 (1): 249–257.

Kong W, Shen B, Lyu H, Kong J, Ma J et al. (2021). Review on carbon dioxide fixation coupled with nutrients removal from wastewater by microalgae. Journal of Cleaner Production 292: 125975. https://doi.org/10.1016/j.jclepro.2021.125975

Kumar K, Banerjee D, Das D (2014). Carbon dioxide sequestration from industrial flue gas by *Chlorella sorokiniana*. Bioresource Technology 152: 225–233. https://doi.org/10.1016/j.biortech.2013.10.098

Langley NM, Harrison STL, van Hille RP. (2012). A critical evaluation of CO_2 supplementation to algal systems by direct injection. Biochemical Engineering Journal, 68: 70–75.

Lara-Gil JA, Senés-Guerrero C, Pacheco A (2016). Cement flue gas as a potential source of nutrients during CO_2 mitigation by microalgae. Algal Research 17: 285–292. https://doi.org/10.1016/j.algal.2016.05.017

LeDuff P, Rorrer GL (2019). Formation of extracellular β-chitin nanofibers during batch cultivation of marine diatom *Cyclotella* sp. at silicon limitation. Journal of Applied Phycology 31 (6): 3479–3490.

Leflay H, Pandhal J, Brown S (2021). Direct measurements of CO_2 capture are essential to assess the technical and economic potential of algal-CCUS. Journal of CO_2 Utilization 52: 101657. https://doi.org/10.1016/j.jcou.2021.101657

Li FF, Yang ZH, Zeng R, Yang G, Chang X et al. (2011). Microalgae capture of CO_2 from actual flue gas discharged from a combustion chamber. Industrial and Engineering Chemistry Research 50 (10): 6496–6502. https://doi.org/10.1021/ie200040q

Lopez PJ, Desclés J, Allen AE, Bowler C (2005). Prospects in diatom research. Current Opinion in Biotechnology 16 (2): 180–186.

Matsuda Y, Hopkinson BM, Nakajima K, Dupont CL, Tsuji Y (2017). Mechanisms of carbon dioxide acquisition and CO_2 sensing in marine diatoms: A gateway to carbon metabolism. Philosophical Transactions B 372 (1728): 20160403 doi:10.1098/rstb.2016.0403

Mansour MP, Frampton DMF, Nichols PD, Volkman JK, Blackburn SI (2005). Lipid and fatty acid yield of nine stationary-phase microalgae: Applications and unusual C24-C28 polyunsaturated fatty acids. Journal of Applied Phycology 17 (4): 287–300.

Martin-Jezequel V, Hildebrand M, Brezinski MA (2000). Silicon metabolism in diatoms: Implications for growth. Journal of Phycology 36: 821–840.

Ozkan A, Rorrer GL (2017a). Effects of CO_2 delivery on fatty acid and chitin nanofiber production during photobioreactor cultivation of the marine diatom *Cyclotella* sp. Algal Research 26: 422–430.

Ozkan A, Rorrer GL (2017b). Effects of light intensity on the selectivity of lipid and chitin nanofiber production during photobioreactor cultivation of the marine diatom *Cyclotella* sp. Algal Research 25: 216–227.

Ozkan A, Rorrer GL (2017c). Lipid and chitin nanofiber production during cultivation of the marine diatom *Cyclotella* sp. to high cell density with multistage addition of silicon and nitrate. Journal of Applied Phycology 29 (4): 1811–1818.

Pashchenko D (2022). Photochemical hydrocarbon fuel regeneration: Hydrogen-rich fuel from CO_2. International Journal of Hydrogen Energy 47 (61): 25531–25540. https://doi.org/10.1016/j.ijhydene.2022.06.002

Rorrer GL (2015). Bioprocess engineering of phototrophic marine organisms. Springer Handbook of Marine Biotechnology. Berlin, Germany: Springler-Verlag.

Ryu K, Rorrer GL (2010). Changes in total lipid contents of marine diatom *Nitzschia frustulum* at various temperature under Si deficiency. Korean Journal of Chemical Engineering 27(2): 567–569.

Sanaye Mozaffari Sabet N, Golzary A (2022). CO_2 biofixation at microalgae photobioreactors: hydrodynamics and mass transfer study. International Journal of Environmental Science and Technology 19(11), 11631–11648. https://doi.org/10.1007/s13762-022-04286-6

Shirazian P, Azin M, Bozorg A (2022). Kinetic models to describe *Nannochloropsis salina* cultivation under different illumination conditions. Environmental Progress and Sustainable Energy e13833. https://doi.org/10.1002/ep.13833

Singh HM, Kothari R, Gupta R, Tyagi VV (2019). Bio-fixation of flue gas from thermal power plants with algal biomass: Overview and research perspectives. Journal of Environmental Management 245: 519–539. https://doi.org/10.1016/j.jenvman.2019.01.043

Singh SP, Singh P (2014). Effect of CO_2 concentration on algal growth: A review. Renewable and Sustainable Energy Reviews 38: 172–179.

Shniukova EI, Zolotareva EK (2015). Diatom exopolysaccharides: A review. International Journal on Algae 17 (1): 50–67.

Sydney EB, Sturm W, de Carvalho JC, Thomaz-Soccol V, Larroche C et al. (2010). Potential carbon dioxide fixation by industrially important microalgae. Bioresource Technology 101 (15): 5892–5896. https://doi.org/10.1016/j.biortech.2010.02.088

Thomas DM, Mechery J, Paulose SV (2016). Carbon dioxide capture strategies from flue gas using microalgae: a review. Environmental Science and Pollution Research 23 (17): 16926–16940. https://doi.org/10.1007/s11356-016-7158-3

Wang C, Lan CQ (2018). Effects of shear stress on microalgae – A review. Biotechnology Advances 36 (4): 986–1002.

Ways P, Hanahan DJ (1964). Characterization and quantification of red cell lipids in normal man. Journal of Lipid Research 5: 318–328.

Zhang X, Lu Z, Wang Y, Wensel P, Sommerfeld M et al. (2016). Recycling *Nannochloropsis oceanica* culture media and growth inhibitors characterization. Algal Research 20: 282–290.

Zhao B, Su Y (2014). Process effect of microalgal-carbon dioxide fixation and biomass production: A review. Renewable and Sustainable Energy Reviews 31: 121–132.

Zhu CJ, Lee YK (1997). Determination of biomass dry weight of marine microalgae. Journal of Applied Phycology 9 (2): 189–194. https://doi.org/10.1023/A:1007914806640